International Journal of Control, Automation and Systems 16(1) (2018) 108-119
http://dx.doi.org/10.1007/s12555-016-0407-x
ISSN:1598-6446 eISSN:2005-4092
http://www.springer.com/12555

Dual-side Event-triggered Output Feedback H_∞ Control for NCS with Communication Delays

Fuqiang Li*, Lisai Gao, Gensheng Dou, and Baozhou Zheng

Abstract: This paper studies the dual-side event-triggered output feedback H_∞ control for networked control system with network-induced delays. Unlike continuous-time event-triggered mechanism (ETM) or state-dependent ETM, the discrete dual-side ETMs are firstly proposed by using plant output and controller output, respectively, which effectively reduce transmission rate of sampled data in both sensor-to-controller and controller-to-actuator channels. Then, the closed-loop system is modelled as a time-delay system, which characterizes effects of the dual-side ETMs and networked-induced delays in a unified framework. Based on the system model, asymptotic stability criterion satisfying H_∞ performance is derived, and conservatism is reduced by the delay decomposition method and reciprocally convex approach. Moreover, a co-design scheme is presented to design the dual-side ETMs and controller simultaneously, which is more convenient than two-step design method requiring controllers to be given a priori. Finally, examples confirm effectiveness of the proposed method.

Keywords: Co-design, dynamic output feedback control, event-triggered mechanism, H_∞ control, networked control system.

1. INTRODUCTION

Networked control system (NCS) is a class of complex dynamical systems wherein the distributed system components, such as sensors, controllers and actuators, are connected through a shared communication network [1]. Due to the advantages of high flexibility, low cost, simple installation and maintenance, NCS has been applied in smart grid, telerobotics, precision agriculture, unmanned aerial vehicles, etc [2, 3].

Typically, the control task in NCS is executed periodically, since this allows the system to be analyzed and synthesized using the well-developed theory on sampled-data systems. To achieve satisfactory control performance even under the worst condition (such as concurrency of delays [4] and dropouts [5]), the sampling period are always set small. However, high sampling frequency may overburden network bandwidth and on-chip battery [6]. To save network bandwidth and energy, event-triggered mechanism (ETM) has been proposed [7], which invokes an information exchange only when event-triggered condition is satisfied. The existing ETMs can be roughly classified into relative ETM and absolute ETM [8]. In the first case, relative ETM uses state-dependent event-triggered threshold. For instance, the ETM in [9] schedules control tasks only when state error norm exceeds weighted state norm, and similars can be seen in [10, 11]. In the second case, absolute ETM uses constant event-triggered threshold. For instance, the ETM in [12] applies impulse control only when state norm equals to a given constant, and similars can be found in [13, 14]. Compared with periodic sampling (time-triggered) method that all sampled data are transmitted, these ETMs can effectively reduce the transmission rate of sampled data, which implies network bandwidth and energy can be saved. Note that these ETMs are state-dependent assuming system state is available. However, full state measurement is often impossible in practice. Besides, these ETMs depend on continuous-time state provided by extra dedicated hardware. However, it is always costly to add hardware to existing systems. Thus, the first motivation is to develop an output based ETM that can be implemented by software.

Manuscript received July 3, 2016; revised December 9, 2016 and April 4, 2017; accepted May 22, 2017. Recommended by Associate Editor M. Chadli under the direction of Editor PooGyeon Park. This work was supported by National Natural Science Foundation of China under grant 61703146, 61673255, Key Scientific and Research Project of the Education Department of Henan Province under grants 16B413002 and 15A510028, Scientific and Technological Project of Henan Province under grant 172102210043 and 162102110108, Scientific and Technological Innovation Project of Henan Agricultural University under grants KJCX2016A09, KJCX2015A17 and KJCX2015A19.

Fuqiang Li is with the College of Sciences, Henan Agricultural University, Zhengzhou 450002, China, and the Shanghai Key Laboratory of Power Station Automation Technology, School of Mechatronics Engineering and Automation, Shanghai University, Shanghai 200072, China (e-mail: fuqiang.li@yahoo.com). Lisai Gao is with the Shanghai Key Laboratory of Power Station Automation Technology, School of Mechatronics Engineering and Automation, Shanghai University, Shanghai 200072, China (e-mail: glsai@126.com). Gensheng Dou and Baozhou Zheng are with the College of Sciences, Henan Agricultural University, Zhengzhou 450002, China (e-mails: dougsh@henau.edu.cn, baozhou120@163.com).
* Corresponding author.

By integrating the ETM into control loop, event-triggered control (ETC) systems are developed. For instance, a simple event-based PID controller is presented in [7], which obtains large reductions in CPU utilization with only minor control performance degradation. An upper bound of the difference between continuous and event-triggered loops is derived in [15], which shows that the approximation of the continuous loop by the ETC loop can be made arbitrarily tight by appropriately choosing parameters of the ETM. The ETC methods for first-order [12], second-order [16] and arbitrary (finite) order systems [17] can guarantee better tradeoffs between control performance and average transmission rate than time-triggered control. A periodic ETC strategy is proposed to strike a balance between the periodic control and the ETC [18]. Using delay system method, state feedback H_∞ control for linear NCS is studied in [19]. Using hybrid systems method, a framework for the event-triggered stabilization of nonlinear systems is proposed in [20], which is general enough to encompass most of the existing ETC techniques. Compared with periodic control system, these ETC systems use less network bandwidth and energy, while guaranteeing satisfactory control performance.

It is worth noting that these ETC systems assume controller and actuator are co-located, and only use the ETM to save network bandwidth in sensor-to-controller (SC) channel. However, controller and actuator may reside on different places [21], which implies it is interesting to employ dual-side ETMs to save network bandwidth in both SC and controller-to-actuator (CA) channels. Besides, these ETC systems use emulation-based (two-step) design method [18], i.e., the controller is firstly designed without considering event-triggered nature of the control system, and, subsequently, an ETM is designed to ensure that the ETC system is stable. Namely, the controller and ETM are designed respectively, which is not convenient. Thus, for the case communication networks exist in both SC and CA channels, how to model the dual-side ETC system, and develop a co-design scheme for dual-side ETMs and controller is the second motivation.

To address the two motivations above, this paper studies the dual-side event-triggered output feedback H_∞ control for NCS with communication delays. The main contributions are: (i) unlike continuous-time state based ETM, the discrete-time output based dual-side ETMs are proposed by using sampled output of the plant and controller at sampling instants, which can be implemented by software. Moreover, the dual-side ETC system is model as a general time-delay system, which characterizes effects of dual-side ETMs and network-induced delays in a unified framework. (ii) unlike the two-step design method requiring controllers to be given a priori, a co-design scheme is introduced to design dual-side ETMs and dynamic output feedback (DOF) controller simultaneously.

The paper is organized as follows. In Section 2, we propose the dual-side ETMs and build the closed-loop system model. System stability is analyzed in Section 3. Sufficient conditions for controller design are provided in Section 4. Examples illustrate the proposed method in Section 5. Section 6 presents the conclusions.

Notation. '*' represents a symmetric term in a symmetric matrix. $\|\cdot\|$ marks the Euclidean norm. I indicates an identity matrix. $\mathrm{Diag}\{X_1,\cdots,X_N\}$ refers to a block-diagonal matrix with entries $X_1,\cdots,X_N$ on the diagonal. $\mathrm{Col}\{X_1,\cdots,X_N\}$ denotes the column vector $[X_1^T,\cdots,X_N^T]^T$.

2. PROBLEM FORMULATION

2.1. System description

Consider a linear time-invariant (LTI) plant

$$\begin{cases} \dot{x}(t) = Ax(t) + Bu(t) + B_\omega \omega(t), \\ y(t) = Cx(t), \\ z(t) = C_1 x(t), \end{cases} \tag{1}$$

where $x(t) \in \mathbb{R}^n$ is state, $u(t) \in \mathbb{R}^{n_u}$ is control input, $\omega(t) \in \mathbb{R}^{n_\omega}$ is disturbance and $\omega(t) \in \mathcal{L}_2[0,\infty)$, $y(t) \in \mathbb{R}^{n_y}$ is measurement output and $z(t) \in \mathbb{R}^{n_z}$ is controlled output, A, B, B_ω, C and C_1 are constant matrices with appropriate dimensions.

As shown in Fig. 1, in SC channel, the sensor samples measurement output of plant with constant sampling period. The ETM determines whether or not sampled output of the plant should be transmitted. The released output of plant arrives at the data processing unit (DPU) through a network with communication delays. The DPU transfers the released output of plant to the zero-order holder (ZOH) using certain timing sequence. The ZOH sends the released output of plant to the DOF controller (DOFC) immediately. By property of the ZOH, the ZOH will hold the released output of plant until the next released output of plant comes.

For convenience of development, some notations are used: $\mathbb{S}_s = \{h, 2h, \ldots\}(k \in \mathbb{N})$ indicates sampling instants of the sensor and the sampler in CA channel, where h is sampling period. $\mathbb{S}_y = \{b_1 h, b_2 h, \ldots\}(b_{k_y} \in \mathbb{N})$ denotes transmission instants of the ETM in SC channel. $\mathbb{S}_u = \{d_1 h, d_2 h, \ldots\}(d_{k_u} \in \mathbb{N})$ marks transmission instants of the ETM in CA channel. In SC channel, plant output released from the ETM at time instant $b_{k_y} h$ will arrive at the DPU

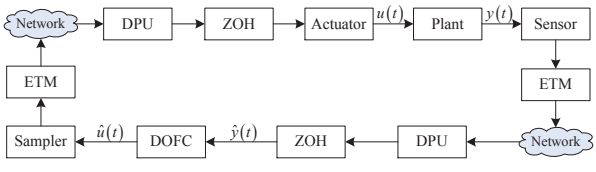

Fig. 1. Framework of the event-triggered NCS.

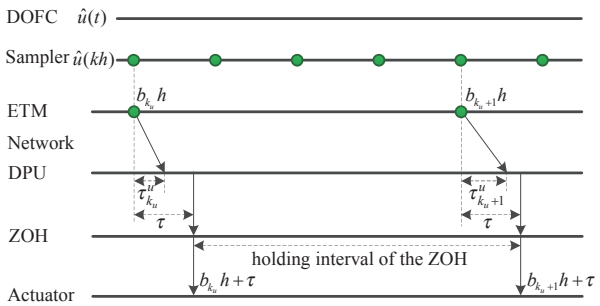

Fig. 2. Time sequence in CA channel.

with network-induced delay $\tau^y_{k_y}$. In CA channel, controller output released from the ETM at time instant $d_{k_u}h$ will arrive at the DPU with network-induced delay $\tau^u_{k_u}$. Without loss of generality, $\tau^y_{k_y}$ and $\tau^u_{k_u}$ are assumed to be upper-bounded, i.e., $0 \le \tau^y_{k_y} \le \tau^y$, $0 \le \tau^u_{k_u} \le \tau^u$. Then, we define the maximum network-induced delay in both SC and CA channels as $\tau := \max\{\tau^y, \tau^u\}$ and focus on the case $\tau < h$ in this paper.

In CA channel, as shown in Fig. 2, the sampler obtains discrete-time output $\hat{u}(kh)$ of the DOF controller. The ETM transmits controller output $\hat{u}(b_{k_u}h)$ only when event-triggered condition is satisfied. The released controller output $\hat{u}(b_{k_u}h)$ arrives at the DPU at time instant $b_{k_u}h+\tau^u_{k_u}$ due to network-induced delay $\tau^u_{k_u}$. The DPU with internal buffer sends the released controller output $\hat{u}(b_{k_u}h)$ to the ZOH at time instant $b_{k_u}h+\tau$. The ZOH immediately transfers the released controller output $\hat{u}(b_{k_u}h)$ to the actuator at time instant $b_{k_u}h+\tau$. By property of the ZOH, the ZOH will hold the latest released controller output $\hat{u}(b_{k_u}h)$ during time interval $[b_{k_u}h+\tau, b_{k_u+1}h+\tau)$ until next controller output $\hat{u}(b_{k_u+1}h)$ arrives at time instant $b_{k_u+1}h+\tau$.

2.2. Event-triggered mechanism

The transmission scheme of the ETM at sensor side is designed as

$$b_{k_y+1}h = b_{k_y}h + \min_{j\in\mathbb{N}}\{jh \,|\, \|\Omega_y^{\frac{1}{2}}[y(b_{k_y}h) - y(b_{k_y}h+jh)]\|^2 \ge \delta_y \|\Omega_y^{\frac{1}{2}} y(b_{k_y}h)\|^2\}, \quad (2)$$

where $0 \le \delta_y < 1$, $\Omega_y > 0$, $y(b_{k_y}h)$ and $y(b_{k_y}h+jh)$ are measurement outputs at the latest transmission instant and current sampling instant, respectively. Min marks the minimum.

The ETM (2) works as follows: since the latest transmission instant $b_{k_y}h$, the ETM checks event-triggered condition $\|\Omega_y^{\frac{1}{2}}[y(b_{k_y}h) - y(b_{k_y}h+jh)]\|^2 \ge \delta_y \|\Omega_y^{\frac{1}{2}} y(b_{k_y}h)\|^2$ at each sampling instant $b_{k_y}h+jh$. If event-triggered condition is satisfied (i.e., an event happens), the sampling instant becomes transmission instant $b_{k_y+1}h$, and sampled output $y(b_{k_y+1}h)$ is transmitted. Otherwise, the data will be discarded.

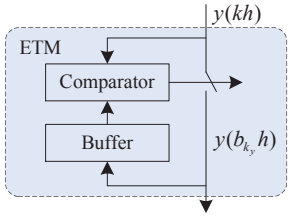

Fig. 3. Structure of the ETM (2).

Unlike periodic sampling mode (i.e., time-triggered mode) that transmits data at each sampling period, the ETM (2) transmits data only when an event happens (i.e., event-triggered condition is satisfied). Thus, transmission instants are subset of sampling instants (i.e., $\mathbb{S}_y \subseteq \mathbb{S}_s$), and system resources such as network bandwidth can be saved.

As shown in Fig. 3, the ETM (2) can be implemented by buffer, comparator and switch. The buffer stores the latest transmitted output $y(b_{k_y}h)$, and it will be updated when next transmitted data $y(b_{k_y+1}h)$ arrives. Since the latest transmission instant $b_{k_y}h$, using sampled output $y(b_{k_y}h+jh)$ from sensor and latest transmitted output $y(b_{k_y}h)$ from buffer, the comparator checks event-triggered condition at each sampling instant $b_{k_y}h+jh$. If event-triggered condition is satisfied (i.e., an event happens), the comparator triggers the switch to turn on and the sampled output is transmitted. Namely, the switch turns on only when event-triggered condition is satisfied and the ETM (2) transmits data only when an event happens.

Specially, when $\delta_y = 0$, the ETM (2) changes into periodic sampling mode, i.e.,

$$b_{k_y+1}h = b_{k_y}h + h. \quad (3)$$

Proof: When $\delta_y = 0$, the ETM (2) becomes

$$b_{k_y+1}h = b_{k_y}h + \min_{j\in\mathbb{N}}\{jh \,|\, \|\Omega_y^{\frac{1}{2}}[y(b_{k_y}h) - y(b_{k_y}h+jh)]\|^2 \ge 0\}. \quad (4)$$

Since Euclidean norm satisfies $\|\cdot\| \ge 0$, the condition $\|\Omega_y^{\frac{1}{2}}[y(b_{k_y}h) - y(b_{k_y}h+jh)]\|^2 \ge 0$ always holds for any $jh (j \in \mathbb{N})$. Thus, it follows from (4) that

$$b_{k_y+1}h = b_{k_y}h + \min_{j\in\mathbb{N}}\{jh\} = b_{k_y}h + h. \quad (5)$$

Due to $b_{k_y+1}h = b_{k_y}h + h$, transmission interval (i.e., $b_{k_y+1}h - b_{k_y}h$) of the ETM equals to sampling period h, which implies the ETM (2) changes into period sampling mode when $\delta_y = 0$. This completes the proof. □

Remark 1: Event-triggered condition of the ETM (2) can also be expressed as $\|\Omega_y^{\frac{1}{2}}[y(b_{k_y}h) - y(b_{k_y}h+jh)]\|^2 / \|\Omega_y^{\frac{1}{2}} y(b_{k_y}h)\|^2 \ge \delta_y$. Namely, once the weighted norm of changing rate of measurement output exceeds a threshold

δ_y, event-triggered condition is satisfied and measurement output is transmitted. Since Ω_y appears in both numerator and denominator, it has little effect on event-triggered condition, but it aims just to enhance the feasibility of the obtained stability criteria [22]. Thus, larger δ_y results in lower transmission rate of the ETM (2). Similar ETM can be found in [9], but it is continuous-time ETM requiring hardware.

Remark 2: Unlike the continuous-time ETMs [9, 20], the ETM (2) has two features: (i) extra hardware is not required to monitor continuous-time plant state, since the ETM (2) is only dependent on measurement output at discrete sampling instants, which implies that the ETM (2) can be implemented by software. (ii) to exclude Zeno behavior [18], complex computation for lower bound of triggering intervals is not needed, since the ETM (2) works at sampling instants, which guarantees that triggering intervals are at least lower bounded by $h > 0$.

Similarly, the transmission scheme of the ETM at the controller side is designed as

$$\begin{aligned} d_{k_u+1}h =& d_{k_u}h + \min_{j\in\mathbb{N}}\{jh \,|\, \|\Omega_u^{\frac{1}{2}}[\hat{u}(d_{k_u}h) \\ & - \hat{u}(d_{k_u}h + jh)]\|^2 \geq \delta_u \|\Omega_u^{\frac{1}{2}}\hat{u}(d_{k_u}h)\|^2\}, \end{aligned} \tag{6}$$

where $0 \leq \delta_u < 1$, $\Omega_u > 0$, $\hat{u}(d_{k_u}h)$ and $\hat{u}(d_{k_u}h + jh)$ are controller output at the latest transmission instant and the current sampling instant, respectively.

Remark 3: The ETM (2) at sensor side and ETM (6) at controller side use local information (plant output or controller output) to decide when to transmit data, thus transmission of one ETM does not necessarily trigger transmission of another ETM. Namely, although the ETMs at both sides may trigger simultaneously, they are not necessarily synchronized. Similar idea can be found in [21].

2.3. Closed-loop system modeling

2.3.1 Modeling in the SC channel

The DPU at sensor side works as follows.

i) The buffer in the DPU receives and stores the latest transmitted data of the ETM at sensor side. Due to networked-induced delay, the data released from the ETM at time instant $b_{k_y}h$ will arrive at the buffer at time instant $b_{k_y}h + \tau_{k_y}^y$, where $\tau_{k_y}^y \leq \tau$.

ii) At each time instant $kh + \tau (k \in \mathbb{N})$, the DPU checks whether or not the buffer has been updated. If yes, the DPU transfers updated data of buffer to ZOH immediately.

Thus, the updating sequence of the ZOH can be described as $\mathbb{S}_{z_y} = \mathbb{S}_y + \tau = \{t_1, t_2, \ldots\}$, where $t_{k_y} = b_{k_y}h + \tau$. By the property of the ZOH, the input signal $\hat{y}(t)$ of the DOF controller can be obtained as

$$\hat{y}(t) = y(b_{k_y}h),\ t \in [t_{k_y}, t_{k_y+1}). \tag{7}$$

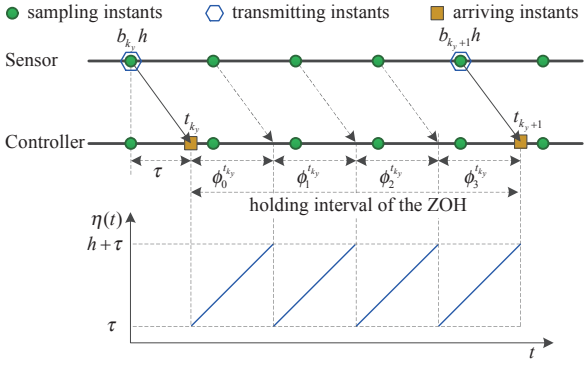

Fig. 4. Division of holding interval of ZOH at sensor side.

Defining $\varepsilon_{k_y} := b_{k_y+1} - b_{k_y} - 1$, the holding interval of the ZOH can be divided as

$$[t_{k_y}, t_{k_y+1}) = \bigcup_{\ell_{k_y}=0}^{\varepsilon_{k_y}} \phi_{\ell_{k_y}}^{t_{k_y}}, \tag{8}$$

where $\phi_{\ell_{k_y}}^{t_{k_y}} = [t_{k_y} + \ell_{k_y}h, t_{k_y} + (\ell_{k_y}+1)h), \ell_{k_y} = 0, 1, \ldots, \varepsilon_{k_y}$. For instance, as shown in Fig. 4, holding interval $[t_{k_y}, t_{k_y+1})$ of the ZOH can be divided into subsets as $\phi_0^{t_{k_y}} = [t_{k_y}, t_{k_y} + h), \phi_1^{t_{k_y}} = [t_{k_y} + h, t_{k_y} + 2h), \phi_2^{t_{k_y}} = [t_{k_y} + 2h, t_{k_y} + 3h)$ and $\phi_3^{t_{k_y}} = [t_{k_y} + 3h, t_{k_y} + 4h)$.

On divided interval $\phi_{\ell_{k_y}}^{t_{k_y}}$, define $\eta(t)$ (as shown in Fig. 4)

$$\eta(t) := t - (b_{k_y}h + \ell_{k_y}h),\ t \in \phi_{\ell_{k_y}}^{t_{k_y}}. \tag{9}$$

$\eta(t)$ is a piecewise-linear function satisfying

$$\tau \leq \eta(t) \leq h + \tau,\ t \in \phi_{\ell_{k_y}}^{t_{k_y}}. \tag{10}$$

Taking time derivative of $\eta(t)$ in (9) yields

$$\dot{\eta}(t) = 1, t \in \phi_{\ell_{k_y}}^{t_{k_y}} \text{ and } t \neq t_{k_y} + \ell_{k_y}h. \tag{11}$$

Proof: Using (8), holding interval $[t_{k_y}, t_{k_y+1})$ of ZOH can be virtually divided into subsets $\phi_{\ell_{k_y}}^{t_{k_y}}$. On artificial-divided subset $\phi_{\ell_{k_y}}^{t_{k_y}}$, $\eta(t)$ is defined as in (9). Then, taking time derivative of $\eta(t)$ in (9) yields

$$\begin{aligned} \dot{\eta}(t) =& \frac{dt}{dt} - \frac{d(b_{k_y}h + \ell_{k_y}h)}{dt} \\ =& 1,\ t \in \phi_{\ell_{k_y}}^{t_{k_y}} \text{ and } t \neq t_{k_y} + \ell_{k_y}h. \end{aligned} \tag{12}$$

This completes the proof. □

Remark 4: As shown in (10), from the analysis view, τ is the minimum value of the function $\eta(t)$, i.e, $\tau \leq \eta(t)$. On the other hand, as shown in Section 2.1, from the practical view, τ denotes the maximum network-induced delay in both SC and CA channels, i.e., $\tau = \max\{\tau^y, \tau^u\}$.

Define piecewise-constant function $e_y(t)$ as $e_y(t) := y(b_{k_y}h) - y(b_{k_y}h + \ell_{k_y}h), t \in \phi_{\ell_{k_y}}^{t_{k_y}}$ [19], i.e.,

$$e_y(t) = \begin{cases} y(b_{k_y}h) - y(b_{k_y}h), & t \in \phi_0^{t_{k_y}}, \\ y(b_{k_y}h) - y(b_{k_y}h + h), & t \in \phi_1^{t_{k_y}}, \\ \vdots & \\ y(b_{k_y}h) - y(b_{k_y}h + \varepsilon_{k_y}h), & t \in \phi_{\varepsilon_{k_y}}^{t_{k_y}}. \end{cases} \tag{13}$$

Using (9) and (13), the controller input in (7) can be described as

$$\hat{y}(t) = e_y(t) + y(t - \eta(t)), \ t \in \phi_{\ell_{k_y}}^{t_{k_y}}. \tag{14}$$

Then, the DOF controller is designed as

$$\begin{cases} \dot{x}_c(t) = A_c x_c(t) + A_{cd} x_c(t - \eta(t)) + B_c \hat{y}(t), \\ \hat{u}(t) = C_c x_c(t), \quad t \in \phi_{\ell_{k_y}}^{t_{k_y}}, \end{cases} \tag{15}$$

where $x_c(t) \in \mathbb{R}^n, \hat{y}(t)$ and $\hat{u}(t)$ denote the state, input and output of the controller, respectively. A_c, A_{cd}, B_c and C_c are gain matrices with appropriate dimensions.

Remark 5: Using $\eta(t)$ in (9), during time interval $t \in \phi_{\ell_{k_y}}^{t_{k_y}} = [b_{k_y} + \ell_{k_y}h + \tau, b_{k_y} + (\ell_{k_y} + 1)h + \tau)$, state $x_c(t - \eta(t)) = x_c(b_{k_y}h + \ell_{k_y}h)$ is history information. Since both history state $x_c(t - \eta(t))$ and current state $x_c(t)$ are employed, the controller (15) is memory controller. As shown in [23], memory controller often achieves good performance, which is the first motivation to design memory controller (15).

On the other hand, using Theorem 2 in Section 4, gain matrices of controller (15) can be obtained in (47), where $A_{cd} = N^{-1}(\Lambda_3 - \Lambda_2 CX - YB\Lambda_1)(I - YX)^{-1}N$. If $A_{cd} = 0$, controller (10) becomes memoryless controller, and we have $\Lambda_3 - \Lambda_2 CX - YB\Lambda_1 = 0$, which is an equality constraint on matrix variables $(\Lambda_1, \Lambda_2, \Lambda_3, X, Y)$. Under this constraint, related matrix inequalities in Theorem 2 are no longer linear, which implies it is difficult to design memoryless controller by LMI technology. Thus, the memory controller (15) is easier to be designed by LMI technology than corresponding memoryless controller, which is the second motivation to design memory controller (15).

As shown in Fig. 4, by dividing the holding interval of the ZOH at the sensor side, the whole operation time can be described as $[t_0, \infty) = \bigcup_{t_{k_y}=t_0}^{t_\infty} \bigcup_{\ell_{k_y}=0}^{\varepsilon_{k_y}} \phi_{\ell_{k_y}}^{t_{k_y}}$. Under the time scale $t \in \phi_{\ell_{k_y}}^{t_{k_y}}$, the controller input $\hat{y}(t)$ is obtained in (14). To build the closed-loop system model, the plant input $u(t)$ in (1) should be described using the same time scale $t \in \phi_{\ell_{k_y}}^{t_{k_y}}$, which is shown in the following.

2.3.2 Modeling in the CA channel

Like the DPU at the sensor side, the DPU at the controller side works as follows: (i) the buffer in the DPU receives and stores the latest transmitted data of the ETM at the controller side. (ii) at each time instant $kh + \tau (k \in \mathbb{N})$, if the buffer is updated, its store will be sent to the ZOH.

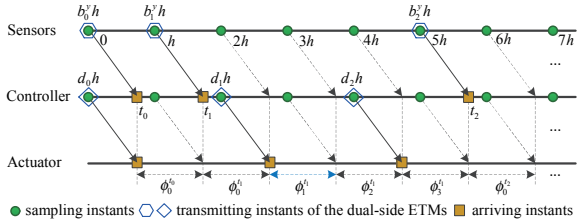

Fig. 5. Division of the whole operation time.

Thus, the updating sequence of the ZOH at the controller side can be denoted by $\mathbb{S}_{z_u} = \mathbb{S}_u + \tau = \{\tau, d_1h + \tau, d_2h + \tau, \ldots\}$, and the control input $u(t)$ of the plant (1) is described as

$$u(t) = \hat{u}(d_{k_u}h), \ t \in [d_{k_u}h + \tau, d_{k_u+1}h + \tau). \tag{16}$$

Like the partition of the holding interval of the ZOH at the sensor side in Fig. 4, the holding interval of the ZOH at the controller side can also be divided equally. Since the updating sequences of the ZOHs at both sides satisfy $\mathbb{S}_{z_y}, \mathbb{S}_{z_u} \subseteq \{\tau, h + \tau, 2h + \tau, \ldots\}$, and their holding intervals are splitted equally, the divided subset for both the ZOHs can be denoted by $\phi_{\ell_{k_y}}^{t_{k_y}}$ as shown in Fig. 5. Obviously, the common time interval $\phi_{\ell_{k_y}}^{t_{k_y}}$ is a subset of one holding interval of the ZOH at the controller side, i.e.,

$$\begin{aligned} \phi_{\ell_{k_y}}^{t_{k_y}} &= [b_{k_y}h + \ell_{k_y}h + \tau, b_{k_y}h + (\ell_{k_y} + 1)h + \tau) \\ &\subseteq [\bar{d}_{k_u}h + \tau, \bar{d}_{k_u+1}h + \tau), \end{aligned} \tag{17}$$

where $\bar{d}_{k_u}h = \max\{d_{k_u}h | d_{k_u}h \le b_{k_y}^y h + \ell_{k_y}h\}$ indicates the latest transmission instant of the ETM at the controller side by the sampling instant $b_{k_y}^y h + \ell_{k_y}h$, and $\bar{d}_{k_u+1}h$ marks the next transmission instant of the ETM after $\bar{d}_{k_u}h$, which implies $\bar{d}_{k_u+1}h \ge b_{k_y}^y h + (\ell_{k_y} + 1)h$. Since the clock is synchronized, the sampling instant $b_{k_y}^y h + \ell_{k_y}h$ is the same for the ETMs at both sides.

Using (17), it follows from (16) that

$$u(t) = \hat{u}(\bar{d}_{k_u}h), \ t \in \phi_{\ell_{k_y}}^{t_{k_y}} \subseteq [\bar{d}_{k_u}h + \tau, \bar{d}_{k_u+1}h + \tau), \tag{18}$$

which implies the plant input $u(t)$ is described using the same time scale $t \in \phi_{\ell_{k_y}}^{t_{k_y}}$ as the controller input $\hat{y}(t)$ in (14). For instance, as shown in Fig. 5, when $t_{k_y} = t_1$ and $\ell_{k_y} = 1$, we have $\phi_{\ell_{k_y}}^{t_{k_y}} = \phi_1^{t_1} = [2h + \tau, 3h + \tau)$. The latest transmission instant of the ETM at the controller side by sampling instant $2h$ is $\bar{d}_{k_u}h = d_1h = 2h$, and the next transmission instant is $\bar{d}_{k_u+1}h = d_2h = 4h$. Then, it is clear that $\phi_1^{t_1} \subseteq [d_1h + \tau, d_2h + \tau) = [2h + \tau, 4h + \tau)$. Since $u(t) = \hat{u}(d_1h), t \in [d_1h + \tau, d_2h + \tau)$, we have $u(t) = \hat{u}(d_1h) = \hat{u}(2h), t \in \phi_1^{t_1}$.

Since $\bar{d}_{k_u}h$ is the latest transmission instant of the ETM at controller side by sampling instant $b_{k_y}h + \ell_{k_y}h$, define

piecewise-constant function $e_u(t)$ as

$$e_u(t) := \hat{u}(\bar{d}_{k_u}h) - \hat{u}(b_{k_y}h + \ell_{k_y}h),\ t \in \phi_{\ell_{k_y}}^{t_{k_y}}. \tag{19}$$

Using (9) and (19), it follows from (18) that

$$u(t) = \hat{u}(\bar{d}_{k_u}h) = e_u(t) + \hat{u}(t-\eta(t)),\ t \in \phi_{\ell_{k_y}}^{t_{k_y}}. \tag{20}$$

Under the time scale $t \in \phi_{\ell_{k_y}}^{t_{k_y}}$, substituting (20) into plant model (1) and using controller model (15), the closed-loop system model is obtained as

$$\begin{cases} \dot{\xi}(t) = \bar{A}\xi(t) + \bar{A}_d\xi(t-\eta(t)) + \bar{B}_y e_y(t) \\ \qquad\quad + \bar{B}_u e_u(t) + \bar{B}_\omega \omega(t), \\ z(t) = \bar{C}_1\xi(t), \quad t \in \phi_{\ell_{k_y}}^{t_{k_y}}, \end{cases} \tag{21}$$

where $\xi(t) = \begin{bmatrix} x(t) \\ x_c(t) \end{bmatrix}, \bar{A} = \begin{bmatrix} A & 0 \\ 0 & A_c \end{bmatrix}, \bar{A}_d = \begin{bmatrix} 0 & BC_c \\ B_cC & A_{cd} \end{bmatrix}, \bar{B}_y = \begin{bmatrix} 0 \\ B_c \end{bmatrix}, \bar{B}_u = \begin{bmatrix} B \\ 0 \end{bmatrix}, \bar{B}_\omega = \begin{bmatrix} B_\omega \\ 0 \end{bmatrix}$ and $\bar{C}_1 = \begin{bmatrix} C_1 & 0 \end{bmatrix}$. The initial condition is supplemented as $\xi(t) = \mathcal{J}(t), t \in [-(h+\tau), 0]$, where $\mathcal{J}(t)$ is a continuous function on $[-(h+\tau), 0]$.

3. STABILITY ANALYSIS OF THE EVENT-TRIGGERED NCS

Based on the closed-loop system model (21), using the Lyapunov-Krasovskii functional approach and linear matrix inequality (LMI) technology [24], system stability will be analyzed in this section.

Lemma 1 [25]**:** Let $f_1, f_2, \ldots, f_N : \mathbb{R}^{\bar{m}} \mapsto \mathbb{R}$ have the positive values in an open subset $\mathbb{D}$ of $\mathbb{R}^{\bar{m}}$. Then, the reciprocally convex combination of f_i over $\mathbb{D}$ satisfies

$$\min \sum_i \frac{1}{\alpha_i} f_i(t) = \sum_i f_i(t) + \max \sum_{i \neq j} g_{i,j}(t), \tag{22}$$

where $\alpha_i > 0, \sum_i \alpha_i = 1$, $g_{i,j} : \mathbb{R}^{\bar{m}} \mapsto \mathbb{R}, g_{j,i}(t) := g_{i,j}(t), \begin{bmatrix} f_i(t) & g_{i,j}(t) \\ g_{i,j}(t) & f_j(t) \end{bmatrix} \geq 0$.

Theorem 1: For given scalars $h > 0, \tau > 0, \gamma > 0$, under the ETM (2) and (6), the system (21) is asymptotically stable with an H_∞ performance index γ for disturbance attenuation, if there exist scalars $0 < \delta_y < 1, 0 < \delta_u < 1$, real matrices $\Omega_y > 0, \Omega_u > 0, P > 0, U > 0, Q > 0, R_i > 0$ $(i = 1,2,3)$, S_2 and S_3 with appropriate dimensions, such that

$$\begin{bmatrix} R_i & * \\ S_i & R_i \end{bmatrix} > 0,\ i = 2,3, \tag{23}$$

$$\begin{bmatrix} \Xi_{11}^i & * \\ \Xi_{21} & \Xi_{22} \end{bmatrix} < 0,\ i = 2,3. \tag{24}$$

Proof: Construct a Lyapunov-Krasovskii functional (LKF) candidate as

$$\begin{aligned} V(t) &= \xi^T(t)P\xi(t) + \int_{t-\eta_1}^{t} \xi^T(s)U\xi(s)ds \\ &\quad + \sum_{i=1}^{3} \eta_{i(i-1)} \int_{-\eta_i}^{-\eta_{i-1}} \int_{t+\theta}^{t} \dot{\xi}^T(s)R_i\dot{\xi}(s)ds d\theta \\ &\quad + \int_{t-\rho}^{t} \zeta^T(s)Q\zeta(s)ds,\ t \in \phi_{\ell_{k_y}}^{t_{k_y}}, \end{aligned} \tag{25}$$

where $P > 0, U > 0, Q > 0, R_i > 0 (i = 1,2,3)$, $\eta_{i(i-1)} = \eta_i - \eta_{i-1}$, $\eta_0 = 0$, $\eta_1 = \tau$, $\eta_3 = h + \tau$, $\rho = \frac{\eta_3 - \eta_1}{2}, \eta_2 = \frac{\eta_3 + \eta_1}{2}$ and $\zeta(t) = \text{col}\{\xi(t-\eta_1), \xi(t-\eta_2)\}$.

Taking the time derivative of $V(t)$ along the trajectory of the closed-loop system (21) yields

$$\begin{aligned} \dot{V}(t) &= sym\{\xi^T(t)P\dot{\xi}(t)\} + \sum_{i=1}^{3} \eta_{i(i-1)}^2 \dot{\xi}^T(t)R_i\dot{\xi}(t) \\ &\quad + \xi^T(t)U\xi(t) - \xi^T(t-\eta_1)U\xi(t-\eta_1) \\ &\quad + \zeta^T(t)Q\zeta(t) - \zeta^T(t-\rho)Q\zeta(t-\rho) \\ &\quad + \sum_{i=1}^{3} \vartheta_i(t),\ t \in \phi_{\ell_{k_y}}^{t_{k_y}}, \end{aligned} \tag{26}$$

where $\vartheta_i(t) = -\eta_{i(i-1)} \int_{t-\eta_i}^{t-\eta_{i-1}} \dot{\xi}^T(\theta)R_i\dot{\xi}(\theta)d\theta$.

Then, two cases are considered.

i) When $\eta(t) \in [\eta_1, \eta_2)$, applying Jensen's inequality [26] to $\vartheta_i(t)$ in (26) yields

$$\begin{aligned} &\vartheta_1(t) \leq \varsigma_1^T R_1 \varsigma_1,\ \vartheta_3(t) \leq \varsigma_3^T R_3 \varsigma_3, \\ &\vartheta_2(t) = -\eta_{21}\Big(\int_{t-\eta(t)}^{t-\eta_1} \varsigma_2 d\theta + \int_{t-\eta_2}^{t-\eta(t)} \varsigma_2 d\theta\Big) \\ &\qquad \leq -\Big(\frac{1}{\alpha_1}\varsigma_4^T R_2 \varsigma_4 + \frac{1}{\alpha_2}\varsigma_5^T R_2 \varsigma_5\Big), \end{aligned} \tag{27}$$

where $\varsigma_1 = x(t) - x(t-\eta_1)$, $\varsigma_3 = x(t-\eta_2) - x(t-\eta_3)$, $\varsigma_2 = \dot{\xi}^T(\theta)R_2\dot{\xi}(\theta)$, $\alpha_1 = \frac{\eta(t)-\eta_1}{\eta_{21}}$, $\alpha_2 = \frac{\eta_2 - \eta(t)}{\eta_{21}}$, $\varsigma_4 = [x(t-\eta_1) - x(t-\eta(t))]$ and $\varsigma_5 = [x(t-\eta(t)) - x(t-\eta_2)]$.

If the condition $\begin{bmatrix} R_2 & * \\ S_2 & R_2 \end{bmatrix} > 0$ in Theorem 1 is satisfied, applying reciprocally convex approach (Lemma 1) to $\vartheta_2(t)$ in (27) yields

$$\vartheta_2(t) \leq -\varsigma_4^T R_2 \varsigma_4 - \varsigma_5^T(t) R_2 \varsigma_5 + sym\{\varsigma_5^T S_2 \varsigma_4\}. \tag{28}$$

ii) Similarly, when $\eta(t) \in [\eta_2, \eta_3]$, use Jensen's inequality to $\vartheta_i(t)$ in (26), and apply reciprocally convex approach to $\vartheta_3(t)$, which is omitted here.

Considering the two cases above, it follows from (26) that

$$\dot{V}(t) \leq \chi^T(t)\Theta^i\chi(t),\ i = 2,3, \tag{29}$$

where $\chi(t) = col\{\xi(t), \xi(t-\eta_1), \xi(t-\eta(t)), \xi(t-\eta_2), \xi(t-\eta_3), e_y(t), e_u(t), \omega(t)\}$, $\Theta^i = sym\{e_1^T P \Gamma_1\} +$

$e_1^TUe_1-e_2^TUe_2+[e_2^T\ e_4^T]Q[e_2^T\ e_4^T]^T-[e_4^T\ e_5^T]Q[e_4^T\ e_5^T]^T+\sum_{j=1}^{3}\eta_{j(j-1)}^2\Gamma_1^TR_j\Gamma_1-(e_1-e_2)^TR_1(e_1-e_2)-(3-i)(e_4-e_5)^TR_3(e_4-e_5)-(3-i)(e_2-e_3)^TR_2(e_2-e_3)-(3-i)(e_3-e_4)^TR_2(e_3-e_4)+(3-i)sym\{(e_3-e_4)^TS_2(e_2-e_3)\}-(i-2)(e_2-e_4)^TR_2(e_2-e_4)-(i-2)(e_4-e_3)^TR_3(e_4-e_3)-(i-2)(e_3-e_5)^TR_3(e_3-e_5)+(i-2)sym\{(e_3-e_5)^TS_3(e_4-e_3)\}$, $\Gamma_1=\bar{A}e_1+\bar{A}_de_3+\bar{B}_ye_6+\bar{B}_ue_7+\bar{B}_\omega e_8$, $e_i=[0_{\bar{n}\times(i-1)\bar{n}}\ I_{\bar{n}}\ 0_{\bar{n}\times(5-i)\bar{n}}\ 0_{\bar{n}\times(n_y+n_u+n_\omega)}]$ $(i=1,\ \ldots,\ 5)$, $e_6=[0_{n_y\times5\bar{n}}\ I_{n_y}\ 0_{n_y\times(n_u+n_\omega)}]$, $e_7=[0_{n_u\times(5\bar{n}+n_y)}\ I_{n_u}\ 0_{n_u\times n_\omega}]$, $e_8=[0_{n_\omega\times(5\bar{n}+n_y+n_u)}\ I_{n_\omega}]$ and $\bar{n}=2n$.

Using the definition of $\eta(t), e_y(t)$ and $e_u(t)$ in (9), (13) and (19), the event-triggered condition in ETM (2) and (6) can be described as

$$\begin{aligned} &e_y^T(t)\Omega_ye_y(t)<\delta_y\psi_y^T\Omega_y\psi_y,\ t\in\phi_{\ell_{k_y}}^{t_{k_y}},\\ &e_u^T(t)\Omega_ue_u(t)<\delta_u\psi_u^T\Omega_u\psi_u,\ t\in\phi_{\ell_{k_y}}^{t_{k_y}}, \end{aligned}\tag{30}$$

where $\psi_y=e_y(t)+y(t-\eta(t))$, $\psi_u=e_u(t)+\hat{u}(t-\eta(t))$.

Obviously, the following equation holds

$$\begin{aligned} \dot{V}(t)=&\dot{V}(t)-e_y^T(t)\Omega_ye_y(t)+e_y^T(t)\Omega_ye_y(t)\\ &-e_u^T(t)\Omega_ue_u(t)+e_u^T(t)\Omega_ue_u(t)\\ &-z^T(t)z(t)+z^T(t)z(t)\\ &-\gamma^2\omega^T(t)\omega(t)+\gamma^2\omega^T(t)\omega(t). \end{aligned}\tag{31}$$

Substituting (29) and (30) into (31) yields

$$\begin{aligned} \dot{V}(t)\le&\chi^T(t)\bar{\Theta}^i\chi(t)-z^T(t)z(t)\\ &+\gamma^2\omega^T(t)\omega(t),\ i=2,3, \end{aligned}\tag{32}$$

where $\bar{\Theta}^i=\Theta^i-e_6^T\Omega_ye_6-e_7^T\Omega_ue_7-\gamma^2e_8^Te_8+\delta_y\Gamma_2^T\Omega_y\Gamma_2+\delta_u\Gamma_3^T\Omega_u\Gamma_3+\Gamma_4^T\Gamma_4, \Gamma_2=CE_1e_3+e_6, \Gamma_3=C_cE_2e_3+e_7, \Gamma_4=\bar{C}_1e_1, E_1=[I_n\ 0]$ and $E_2=[0\ I_n]$.

$\bar{\Theta}^i$ in (32) can be expressed as

$$\bar{\Theta}^i=\Xi_{11}^i-\Xi_{21}^T\Xi_{22}^{-1}\Xi_{21},\ i=2,3,\tag{33}$$

where $\Xi_{11}^i=\Theta^i-\sum_{j=1}^{3}\eta_{j(j-1)}^2\Gamma_1^TR_j\Gamma_1-e_6^T\Omega_ye_6-e_7^T\Omega_ue_7-\gamma^2e_8^Te_8$, $\Xi_{21}=\mathrm{col}\{\Gamma_2,\Gamma_3,\eta_1\Gamma_1,\eta_{21}\Gamma_1,\eta_{32}\Gamma_1,\Gamma_4\}$, $\Xi_{22}=diag\{-\delta_y^{-1}\Omega_y^{-1},-\delta_u^{-1}\Omega_u^{-1},-R_1^{-1},-R_2^{-1},-R_3^{-1},-I\}$.

If the condition $\begin{bmatrix}\Xi_{11}^i & *\\ \Xi_{21} & \Xi_{22}\end{bmatrix}<0$ in Theorem 1 is satisfied, using Schur complement [27] yields

$$\Xi_{11}^i-\Xi_{21}^T\Xi_{22}^{-1}\Xi_{21}<0,\ i=2,3,\tag{34}$$

which implies $\bar{\Theta}^i<0 (i=2,3)$ using (33).

Thus, from (32) and (34), one can derive that: if conditions in Theorem 1 are satisfied, the system (21) with $\omega(t)=0$ is asymptotically stable, and $\|z(t)\|<\gamma\|\omega\|$ under the zero initial condition. This completes the proof. □

Remark 6: By dividing interval $\eta(t)\in[\eta_1,\eta_3]$ into $[\eta_1,\eta_2)$ and $[\eta_2,\eta_3]$, where $\eta_2=\frac{\eta_1+\eta_3}{2}$, delay decomposition method is used to construct the LKF (25), which contains η_2-dependent terms $\eta_{21}\int_{-\eta_2}^{-\eta_1}\int_{t+\theta}^{t}\dot{\xi}^T(s)R_2\dot{\xi}(s)dsd\theta$ and $\eta_{32}\int_{-\eta_3}^{-\eta_2}\int_{t+\theta}^{t}\dot{\xi}^T(s)R_3\dot{\xi}(s)dsd\theta$. Then, as shown in (28), reciprocally convex approach is used to handle second-order integral terms in proof of Theorem 1. As shown in [28] and [25], delay decomposition method and reciprocally convex approach help reduce conservatism. Thus, low conservatism of Theorem 1 can be expected.

As a special case, if the ETM and network only exist at the sensor side, the system (21) changes into

$$\begin{cases} \dot{\xi}(t)=\tilde{A}\xi(t)+\tilde{A}_d\xi(t-\eta(t))+\bar{B}_ye_y(t)\\ \qquad\qquad +\bar{B}_\omega\omega(t),\\ z(t)=\bar{C}_1\xi(t),\ t\in\phi_{\ell_{k_y}}^{t_{k_y}}, \end{cases}\tag{35}$$

where $\tilde{A}=\begin{bmatrix}A & BC_c\\ 0 & A_c\end{bmatrix}$ and $\tilde{A}_d=\begin{bmatrix}0 & 0\\ B_cC & A_{cd}\end{bmatrix}$.

Corollary 1: For given scalars $h>0, \tau>0, \gamma>0$, under the ETM (2), the system (35) is asymptotically stable with an H_∞ performance index γ for disturbance attenuation, if there exists scalar $0<\delta_y<1$, real matrices $\Omega_y>0, P>0, U>0, Q>0, R_i>0 (i=1,2,3)$, S_2 and S_3 with appropriate dimensions, such that

$$\begin{bmatrix}R_i & *\\ S_i & R_i\end{bmatrix}>0,\ i=2,3,\tag{36}$$

$$\begin{bmatrix}\tilde{\Xi}_{11}^i & *\\ \tilde{\Xi}_{21} & \tilde{\Xi}_{22}\end{bmatrix}<0,\ i=2,3.\tag{37}$$

Proof: Like the proof of Theorem 1, constructing a LKF candidate (25), and taking time derivative of the LKF (25) along trajectory of the system (35), we have

$$\dot{V}(t)\le\tilde{\chi}^T(t)\tilde{\Theta}^i\tilde{\chi}(t),\ i=2,3\tag{38}$$

where $\tilde{\chi}(t)=col\{\xi(t),\xi(t-\eta_1),\xi(t-\eta(t)),\xi(t-\eta_2),\xi(t-\eta_3),e_y(t),\omega(t)\}$, $\tilde{\Theta}^i=sym\{\tilde{e}_1^TP\tilde{\Gamma}_1\}+\tilde{e}_1^TU\tilde{e}_1-\tilde{e}_2^TU\tilde{e}_2+[\tilde{e}_2^T\ \tilde{e}_4^T]Q[\tilde{e}_2^T\ \tilde{e}_4^T]^T-[\tilde{e}_4^T\ \tilde{e}_5^T]Q[\tilde{e}_4^T\ \tilde{e}_5^T]^T+\sum_{j=1}^{3}\eta_{j(j-1)}^2\tilde{\Gamma}_1^TR_j\tilde{\Gamma}_1-(\tilde{e}_1-\tilde{e}_2)^TR_1(\tilde{e}_1-\tilde{e}_2)-(3-i)(\tilde{e}_4-\tilde{e}_5)^TR_3(\tilde{e}_4-\tilde{e}_5)-(3-i)(\tilde{e}_2-\tilde{e}_3)^TR_2(\tilde{e}_2-\tilde{e}_3)-(3-i)(\tilde{e}_3-\tilde{e}_4)^TR_2(\tilde{e}_3-\tilde{e}_4)+(3-i)sym\{(\tilde{e}_3-\tilde{e}_4)^TS_2(\tilde{e}_2-\tilde{e}_3)\}-(i-2)(\tilde{e}_2-\tilde{e}_4)^TR_2(\tilde{e}_2-\tilde{e}_4)-(i-2)(\tilde{e}_4-\tilde{e}_3)^TR_3(\tilde{e}_4-\tilde{e}_3)-(i-2)(\tilde{e}_3-\tilde{e}_5)^TR_3(\tilde{e}_3-\tilde{e}_5)+(i-2)sym\{(\tilde{e}_3-\tilde{e}_5)^TS_3(\tilde{e}_4-\tilde{e}_3)\}, \tilde{\Gamma}_1=\tilde{A}e_1+\tilde{A}_de_3+\bar{B}_ye_6+\bar{B}_\omega e_7$, $\tilde{e}_i=[0_{\bar{n}\times(i-1)\bar{n}}\ I_{\bar{n}}\ 0_{\bar{n}\times(5-i)\bar{n}}\ 0_{\bar{n}\times(n_y+n_\omega)}]$ $(i=1,\ \ldots,5)$, $\tilde{e}_6=[0_{n_y\times5\bar{n}}\ I_{n_y}\ 0_{n_y\times n_\omega}]$ and $\tilde{e}_7=[0_{n_\omega\times(5\bar{n}+n_y)}\ I_{n_\omega}]$.

Like (30), the event-triggered condition in ETM (2) can be described as

$$e_y^T(t)\Omega_ye_y(t)<\delta_y\psi_y^T\Omega_y\psi_y,\ t\in\phi_{\ell_{k_y}}^{t_{k_y}},\tag{39}$$

where $\psi_y=e_y(t)+y(t-\eta(t))$.

Obviously, the following equation holds

$$\begin{aligned} \dot{V}(t)=&\dot{V}(t)-e_y^T(t)\Omega_ye_y(t)+e_y^T(t)\Omega_ye_y(t)\\ &-z^T(t)z(t)+z^T(t)z(t) \end{aligned}$$

Table 1. Upper bound of η_3 under different value of η_1.

Methods \ η_1	0	0.1	0.2	0.3	0.4	0.5
Proposition 4 in [29]	1.55	1.62	1.69	1.75	1.81	1.86
Corollary 1	1.89	1.95	2.01	2.06	2.10	2.13

$$-\gamma^2\omega^T(t)\omega(t)+\gamma^2\omega^T(t)\omega(t). \tag{40}$$

Substituting (38) and (39) into (40) yields

$$\begin{aligned}\dot{V}(t) \le & \chi^T(t)\hat{\Theta}^i\chi(t)-z^T(t)z(t)\\ & +\gamma^2\omega^T(t)\omega(t),\ i=2,3,\end{aligned} \tag{41}$$

where $\hat{\Theta}^i = \tilde{\Theta}^i - \tilde{e}_6^T\Omega_y\tilde{e}_6 - \gamma^2\tilde{e}_7^T\tilde{e}_7 + \delta_y\tilde{\Gamma}_2^T\Omega_y\tilde{\Gamma}_2 + \tilde{\Gamma}_3^T\tilde{\Gamma}_3, \tilde{\Gamma}_2 = CE_1\tilde{e}_3+\tilde{e}_6$ and $\tilde{\Gamma}_3 = \bar{C}_1\tilde{e}_1$.

$\hat{\Theta}^i$ in (41) can also be expressed as

$$\hat{\Theta}^i = \tilde{\Xi}_{11}^i - \tilde{\Xi}_{21}^T\tilde{\Xi}_{22}^{-1}\tilde{\Xi}_{21},\ i=2,3, \tag{42}$$

where $\tilde{\Xi}_{11}^i = \tilde{\Theta}^i - \sum_{j=1}^3\eta_{j(j-1)}^2\tilde{\Gamma}_1^TR_j\tilde{\Gamma}_1 - \tilde{e}_6^T\Omega_y\tilde{e}_6 - \gamma^2\tilde{e}_7^T\tilde{e}_7$, $\tilde{\Xi}_{21} = \text{col}\{\tilde{\Gamma}_2, \eta_1\tilde{\Gamma}_1, \eta_{21}\tilde{\Gamma}_1, \eta_{32}\tilde{\Gamma}_1, \tilde{\Gamma}_3\}$ and $\tilde{\Xi}_{22} = diag\{-\delta_y^{-1}\Omega_y^{-1}, -R_1^{-1}, -R_2^{-1}, -R_3^{-1}, -I\}$.

If the condition $\begin{bmatrix}\tilde{\Xi}_{11}^i & * \\ \tilde{\Xi}_{21} & \tilde{\Xi}_{22}\end{bmatrix} < 0$ in Corollary 1 is satisfied, using Schur complement yields

$$\tilde{\Xi}_{11}^i - \tilde{\Xi}_{21}^T\tilde{\Xi}_{22}^{-1}\tilde{\Xi}_{21} < 0,\ i=2,3, \tag{43}$$

which implies $\hat{\Theta}^i < 0 (i=2,3)$ using (42).

Thus, from (41) and (43), one can derive that: if conditions in Corollary 1 are satisfied, the system (35) with $\omega(t)=0$ is asymptotically stable, and $\|z(t)\| < \gamma\|\omega\|$ under the zero initial condition. This completes the proof. □

Remark 7: Using the satellite system in [29], Table 1 lists the upper bound of η_3 under different value of η_1. Due to the usage of delay decomposition method and reciprocally convex approach, Corollary 1 obtains bigger upper bound of η_3 than Proposition 4 in [29]. Thus, Corollary 1 has lower conservatism, which confirms Remark 6.

Since gain matrices (A_c, A_{cd}, B_c, C_c) of the controller (15) are coupled with positive matrix P in Theorem 1, they can not be computed directly. To this end, we will present sufficient conditions for controller design in the following section.

4. CO-DESIGN OF THE ETM AND CONTROLLER

Lemma 2 [30]**:** For matrices $R>0, X$ and any scalar σ, the following inequality holds

$$-XR^{-1}X \le \sigma^2R - 2\sigma X \tag{44}$$

Theorem 2: For given scalars $h>0, \tau>0, \gamma>0$, if there exist scalars $\bar{\delta}_y > 1, \bar{\delta}_u > 1$, real matrices $\Omega_y > 0, \Omega_u > 0, \bar{U} > 0, \bar{Q} > 0, \bar{R}_i > 0 (i=1,2,3), Z = \begin{bmatrix}X & * \\ I & Y\end{bmatrix} > 0$, $\bar{S}_2$ and $\bar{S}_3$ with appropriate dimensions, satisfying

$$\begin{bmatrix}\bar{R}_i & * \\ \bar{S}_i & \bar{R}_i\end{bmatrix} > 0,\ i=2,3, \tag{45}$$

$$\begin{bmatrix}\bar{\Xi}_{11}^i & * \\ \bar{\Xi}_{21} & \bar{\Xi}_{22}\end{bmatrix} < 0,\ i=2,3, \tag{46}$$

then under the ETM (2) and (6), the system (21) is asymptotically stable with an H_∞ performance index γ for disturbance attenuation, and gain matrices of the controller (15) are obtained as

$$\begin{aligned}A_c &= N^{-1}(\Lambda_4 - YAX)(I-YX)^{-1}N,\\ A_{cd} &= N^{-1}(\Lambda_3 - \Lambda_2CX - YB\Lambda_1)(I-YX)^{-1}N\\ B_c &= N^{-1}\Lambda_2,\ C_c = \Lambda_1(I-YX)^{-1}N.\end{aligned} \tag{47}$$

Proof: Partition matrix P as

$$P = \begin{bmatrix}Y & * \\ N^T & N^T(Y-X^{-1})^{-1}N\end{bmatrix}, \tag{48}$$

where matrices $X, Y, N \in \mathbb{R}^{n\times n}$. If matrix N is singular, then there exists sufficiently small scalar $\varepsilon > 0$, such that $N + \varepsilon \times I$ is non-singular and $P + \varepsilon \times \begin{bmatrix}0 & I \\ I & 0\end{bmatrix}$ also satisfies the conditions of Theorem 1. Thus, without loss of generality, matrix N is supposed to be non-singular.

Applying Schur complement to (48) yields

$$P>0 \Leftrightarrow \begin{cases}Y - X^{-1} > 0\\ X > 0\end{cases} \Leftrightarrow Z = \begin{bmatrix}X & * \\ I & Y\end{bmatrix} > 0. \tag{49}$$

Define matrices Ψ_1 and Ψ_2 as

$$\begin{aligned}\Psi_1 &= \begin{bmatrix}X & I \\ N^{-1}(I-YX) & 0\end{bmatrix},\\ \Psi_2 &= P\Psi_1 = \begin{bmatrix}I & Y \\ 0 & N^T\end{bmatrix}.\end{aligned} \tag{50}$$

Define matrices Υ_1 and Υ_2 as

$$\begin{aligned}\Upsilon_1 &= \text{diag}\{\Psi_1, \Psi_1\},\\ \Upsilon_2 &= \text{diag}\{\Upsilon_1, \Upsilon_1, \Psi_1, I, I, I, I, I, \Psi_2, \Psi_2, \Psi_2, I\}.\end{aligned} \tag{51}$$

Using (51), perform congruence transformations to conditions in Theorem 1 as

$$\begin{aligned}&\begin{bmatrix}\bar{R}_i & * \\ \bar{S}_i & \bar{R}_i\end{bmatrix} = \Upsilon_1^T\begin{bmatrix}R_i & * \\ S_i & R_i\end{bmatrix}\Upsilon_1 > 0,\ i=2,3,\\ &\begin{bmatrix}\bar{\Xi}_{11}^i & * \\ \bar{\Xi}_{21} & \hat{\Xi}_{22}\end{bmatrix} = \Upsilon_2^T\begin{bmatrix}\Xi_{11}^i & * \\ \Xi_{21} & \Xi_{22}\end{bmatrix}\Upsilon_2 < 0,\ i=2,3,\end{aligned} \tag{52}$$

where $\bar{\Xi}_{11}^i = sym\{e_1^T\bar{\Gamma}_1\} + e_1^T\bar{U}e_1 - e_2^T\bar{U}e_2 + [e_2^T \ e_4^T]\bar{Q}[e_2^T \ e_4^T]^T - [e_4^T \ e_5^T]\bar{Q}[e_4^T \ e_5^T]^T - (e_1-e_2)^T\bar{R}_1(e_1-e_2) - (3-i)(e_4-e_5)^T\bar{R}_3(e_4-e_5) - (3-i)(e_2-e_3)^T\bar{R}_2(e_2-e_3) - (3-i)(e_3-e_4)^T\bar{R}_2(e_3-e_4) + (3-i)sym\{(e_3-e_4)^T\bar{S}_2(e_2-e_3)\} - (i-2)(e_2-e_4)^T\bar{R}_2(e_2-e_4) - (i-2)(e_4-e_3)^T\bar{R}_3(e_4-e_3) - (i-2)(e_3-e_5)^T\bar{R}_3(e_3-e_5) + (i-2)sym\{(e_3-e_5)^T\bar{S}_3(e_4-e_3)\} - e_6^T\Omega_y e_6 - e_7^T\Omega_u e_7 - \gamma^2 e_8^T e_8$, $\bar{\Xi}_{21} = col\{\bar{\Gamma}_2, \bar{\Gamma}_3, \eta_1\bar{\Gamma}_1, \eta_{21}\bar{\Gamma}_1, \eta_{32}\bar{\Gamma}_1, \bar{\Gamma}_4\}$, $\hat{\Xi}_{22} = diag\{-\delta_y^{-1}\Omega_y^{-1}, -\delta_u^{-1}\Omega_u^{-1}, -Z\bar{R}_1^{-1}Z, -Z\bar{R}_2^{-1}Z, -Z\bar{R}_3^{-1}Z, -I\}$, $\bar{\Gamma}_1 = \phi_1 e_1 + \phi_2 e_3 + \phi_3 e_6 + \phi_4 e_7 + \phi_5 e_8$, $\bar{\Gamma}_2 = \phi_6 e_3 + e_6$, $\bar{\Gamma}_3 = \phi_7 e_3 + e_7$, $\bar{\Gamma}_4 = \phi_8 e_1$, $\phi_1 = \begin{bmatrix} AX & A \\ \Lambda_4 & YA \end{bmatrix}$, $\phi_2 = \begin{bmatrix} B\Lambda_1 & 0 \\ \Lambda_3 & \Lambda_2 C \end{bmatrix}$, $\phi_3 = \begin{bmatrix} 0 \\ \Lambda_2 \end{bmatrix}$, $\phi_4 = \begin{bmatrix} B \\ YB \end{bmatrix}$, $\phi_5 = \begin{bmatrix} B_\omega \\ YB_\omega \end{bmatrix}$, $\phi_6 = \begin{bmatrix} CX & C \end{bmatrix}$, $\phi_7 = \begin{bmatrix} \Lambda_1 & 0 \end{bmatrix}$, $\phi_8 = \begin{bmatrix} C_1 X & C_1 \end{bmatrix}$, $\bar{U} = \Psi_1^T U \Psi_1$, $\bar{Q} = \Upsilon_1^T Q \Upsilon_1$, $\bar{R}_i = \Psi_1^T R_i \Psi_1$ $(i = 1, 2, 3)$, $\bar{S}_i = \Psi_1^T S_i \Psi_1$ $(i = 2, 3)$, $\Lambda_1 = C_c N^{-1}(I - YX)$, $\Lambda_2 = NB_c$, $\Lambda_3 = \Lambda_2 CX + YB\Lambda_1 + NA_{cd}N^{-1}(I - YX)$ and $\Lambda_4 = YAX + NA_c N^{-1}(I - YX)$.

Using Lemma 2 with $\sigma = 1$ to decouple nonlinear terms in $\hat{\Xi}_{22}$ in (52) yields

$$\begin{aligned}\bar{\Xi}_{22} =& \text{diag}\{\Omega_y - 2\bar{\delta}_y I, \Omega_u - 2\bar{\delta}_u I, \bar{R}_1 - 2Z, \\ & \bar{R}_2 - 2Z, \bar{R}_3 - 2Z, -I\},\end{aligned} \tag{53}$$

where $\bar{\delta}_y = \delta_y^{-\frac{1}{2}}$ and $\bar{\delta}_u = \delta_u^{-\frac{1}{2}}$. This completes the proof. □

To deal with the unknown matrix N in (47), applying an irreducible linear transformation $x_c(t) = N^{-1}\bar{x}_c(t)$ to the controller (15), an equivalent controller is obtained as

$$\begin{cases} \dot{\bar{x}}_c(t) = \bar{A}_c\bar{x}_c(t) + \bar{A}_{cd}\bar{x}_c(t - \eta(t)) + \bar{B}_c\hat{y}(t), \\ \hat{u}(t) = \bar{C}_c\bar{x}_c(t), \quad t \in \phi_{\ell_{k_y}}^{t_{k_y}}, \end{cases} \tag{54}$$

where

$$\begin{aligned} \bar{A}_c &= (\Lambda_4 - YAX)(I - YX)^{-1}, \\ \bar{A}_{cd} &= (\Lambda_3 - \Lambda_2 CX - YB\Lambda_1)(I - YX)^{-1}, \\ \bar{B}_c &= \Lambda_2, \ \bar{C}_c = \Lambda_1(I - YX)^{-1}. \end{aligned} \tag{55}$$

Remark 8: Since gain matrices (A_c, A_{cd}, B_c, C_c) of the controller (15) are coupled with positive matrix P, Theorem 1 can only be used to check system stability with given controller, but can not be directly used to design controller. To this end, by decoupling nonlinear terms in Theorem 1, Theorem 2 provides sufficient conditions for event-triggered controller design, and the designed controller (54) is equivalent to controller (15) in Theorem 1.

Remark 9: Event-triggered control system has also been studied by impulsive system method [31] and passive approach [32], and both of them use two-step design method requiring controllers to be given a priori. However, using Theorem 2, parameters of the ETM (2) and (6), and gain matrices of the controller (54) can be achieved simultaneously. Namely, Theorem 2 provides a co-design scheme to design the ETM and controller simultaneously, which is more convenient than two-step design method.

5. EXAMPLES

To illustrate advantages of the ETM (2) and (6), the satellite system in [29] is used, and its state-space representation can be given by the LTI system (1) with

$$A = \begin{bmatrix} 0 & 1 & 0 & 0 \\ -\frac{k}{J_2} & -\frac{d}{J_2} & \frac{k}{J_2} & \frac{d}{J_2} \\ 0 & 0 & 0 & 1 \\ \frac{k}{J_1} & \frac{d}{J_1} & -\frac{k}{J_1} & -\frac{d}{J_1} \end{bmatrix}, \ B = \begin{bmatrix} 0 \\ 0 \\ 0 \\ \frac{1}{J_1} \end{bmatrix}.$$

Setting $J_1 = J_2 = 1, k = 0.09, d = 0.0219$, since the eigenvalues of A are $-0.0219 + 0.4237j, -0.0219 - 0.4237j, 0$ and 0, the system is unstable. Other parameters are set as: $C = \begin{bmatrix} 0 & 0 & 1 & 0 \\ 1 & 0 & 1 & 0 \end{bmatrix}$, $B_\omega = 0.01\text{col}\{1,1,1,1\}$, $C_1 = [0 \ 0 \ 0 \ 1]$, $\omega(t) = 2\sin(2\pi t)$, $h = 10\text{ms}, \tau = 2\text{ms}$ and $\gamma = 25$. Initial conditions of satellite system and controller (54) are $x_0 = \text{col}\{0.2, -0.3, 0.3, -0.2\}$ and $\bar{x}_{c0} = \mathbf{0}$, respectively. Simulation time is $t_s = 90\text{s}$.

Using Theorem 2 to compute parameters of the ETM (2) and ETM (6), and gain matrices of controller (54) simultaneously yields: $\delta_y = 3.16 \times 10^{-5}, \Omega_y = \begin{bmatrix} 244.17 & -55.07 \\ -55.07 & 135.16 \end{bmatrix}, \delta_u = 1.64 \times 10^{-5}, \Omega_u = 476.23,$

$$\bar{A}_c = \begin{bmatrix} 0.3047 & 0.1374 & 0.1044 & -0.1760 \\ -0.9538 & 0.0168 & 0.2659 & -0.9091 \\ 0.0749 & -0.0132 & 0.4702 & 0.6297 \\ 0.0138 & -0.0170 & -0.9036 & -0.8317 \end{bmatrix},$$

$$\bar{A}_{cd} = \begin{bmatrix} -0.3496 & -0.0631 & -0.2799 & -0.0835 \\ -0.3080 & -0.2245 & -2.5239 & -1.6414 \\ 0.0320 & 0.0094 & 0.4480 & 0.5102 \\ -0.2798 & -0.2029 & -2.3035 & -1.5125 \end{bmatrix},$$

$$\bar{B}_c = \begin{bmatrix} 53.5601 & -49.0680 \\ -4.4032 & 0.9791 \\ -31.7917 & 4.0164 \\ -1.8227 & 0.5953 \end{bmatrix} \text{ and } \bar{C}_c = \begin{bmatrix} 0.0007 \\ 0.0005 \\ 0.0058 \\ 0.0038 \end{bmatrix}^T.$$

As shown in Fig. 6 and Fig. 7, the satellite system under the dual-side ETM can be stabilized, and the performance of event-triggered control is very similar to that of periodic sampling control. Actual disturbance attenuation rate of the event-triggered control system is obtained as $\bar{\gamma} = 19.8$ satisfying $\bar{\gamma} < \gamma$, which implies H_∞ performance is guaranteed.

As a performance index, transmission rate of the ETM is defined as $r_t = \frac{n_t}{n_s} \times 100\%$, where n_t and n_s denote numbers of transmitted data and sampled data, respectively. Using simulation time $t_s = 90s$ and sampling pe-

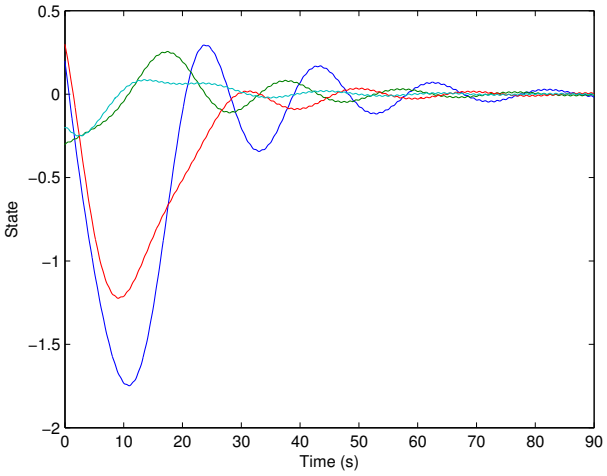

Fig. 6. State responses under the dual-side ETM.

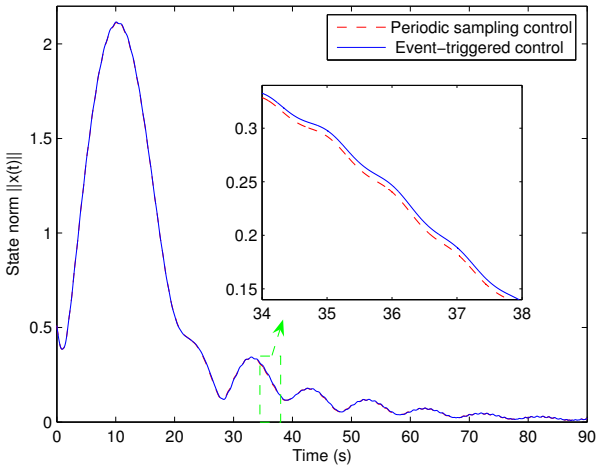

Fig. 7. Evolution of state norm $\|x(t)\|$.

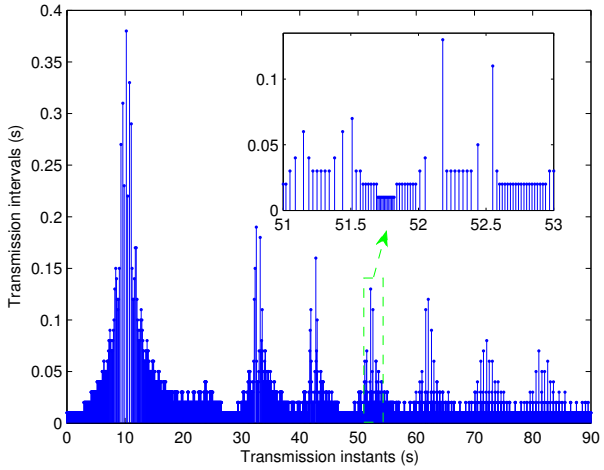

Fig. 8. Transmission instants and transmission intervals of ETM at sensor side.

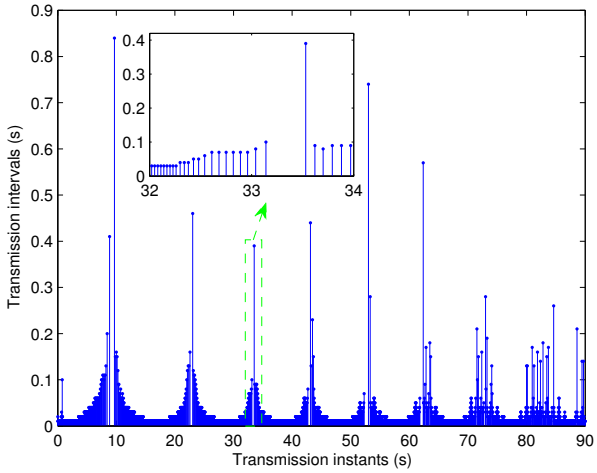

Fig. 9. Transmission instants and transmission intervals of ETM at controller side.

riod $h = 0.01s$, number of sampled data in both SC and CA channels can be obtained as $n_s = \frac{t_s}{h} = 9000$.

Fig. 8 describes transmission instants and transmission intervals of the ETM (2) at sensor side, where transmission interval indicates time interval between two consecutive transmission instants. In Fig. 8, number of transmission instants (i.e., number of transmitted plant output) is $n_t = 5490$. Thus, transmission rate of the ETM (2) is $r_t = \frac{n_t}{n_s} \times 100\% = 61\%$. Compared with periodic sampling scheme that all sampled data are transmitted (i.e., $r_t = 100\%$), 39% networked bandwidth in SC channel can be saved by the ETM (2) at sensor side.

Similarly, Fig. 9 shows transmission instants and transmission intervals of the ETM (6) at controller side. The number of transmission instants (i.e., number of transmitted controller output) is $n_t = 5256$, and thus transmission rate of the ETM (6) can be achieved as $r_t = 58\%$. Compared with periodic sampling scheme, 42% networked bandwidth in CA channel can be saved by the ETM (6) at controller side.

From Figs. 6-9, one can observe that the event-triggered control system using the dual-side ETM can save network bandwidths in both SC and CA channels while guaranteeing satisfactory control performance.

Remark 10: If the ETM and network only exist at sensor side, based on Corollary 1, using the satellite system above with $h = 0.1$s, $\tau = 0.05$s, $t_s = 60$s and $\omega(t) = 0$, Table 2 lists transmission rate of the ETM (2) under different threshold δ_y. When δ_y increases, transmission rate of the ETM (2) decreases, which confirms Remark 1. Besides, as shown in (3), when $\delta_y = 0$, the ETM (2) becomes periodic sampling mode, which implies transmission rate is $r_t = 100\%$. In this case, Ω_y has no effect on the ETM (2) and transmission rate r_t, and thus its value is omitted in Table 2.

Table 2. Transmission rate of ETM (2) under different δ_y.

δ_y	0	0.002	0.004	0.006	0.008	0.01
Ω_y	-	$\begin{bmatrix} 4.2 & 2.3 \\ 2.3 & 12.0 \end{bmatrix}$	$\begin{bmatrix} 3.3 & 1.8 \\ 1.8 & 9.0 \end{bmatrix}$	$\begin{bmatrix} 2.6 & 1.3 \\ 1.3 & 7.2 \end{bmatrix}$	$\begin{bmatrix} 2.2 & 0.9 \\ 0.9 & 6.0 \end{bmatrix}$	$\begin{bmatrix} 2.3 & 1.2 \\ 1.2 & 5.9 \end{bmatrix}$
$r_t(\%)$	100	43.5	32.7	24.5	22.3	20.8

6. CONCLUSION

The dual-side event-triggered output feedback H_∞ control for NCS with communication delays is studied in this paper. Firstly, the discrete dual-side ETMs are proposed by using outputs of plant and controller, respectively, which effectively reduce transmission rate of sampled data in both SC and CA channels. Since the dual-side ETMs work at discrete sampling instants, it can be easily implemented by software, and Zeno behavior can be excluded. Then, the closed-loop time-delay system model is established, which integrates parameters of the dual-side ETMs, network-induced delays, plant and controller dynamics in a unified framework. Sufficient conditions for system asymptotic stability with guaranteed H_∞ performance are obtained, and the conservatism is reduced by the delay decomposition method and reciprocally convex approach. Moreover, sufficient condition for event-triggered controller design is presented, which can compute parameters of the dual-side ETMs and gain matrices of the DOF controller simultaneously. Namely, the ETMs and controller can be co-designed, which is more convenient than the two-step design method.

REFERENCES

[1] Y. Wang, J. Lu, Z. Li, and Y. Chu, "Mixed H_2/H_∞ control for a class of nonlinear networked control systems," *International Journal of Control, Automation and Systems*, vol. 14, no. 3, pp. 655-665, June 2016. [click]

[2] R. Wang, H. Jing, J. Wang, M. Chadli, and N. Chen, "Robust output-feedback based vehicle lateral motion control considering network-induced delay and tire force saturation," *Neurocomputing*, vol. 214, pp. 409-419, November 2016. [click]

[3] C. Peng and J. Zhang, "Delay-distribution-dependent load frequency control of power systems with probabilistic interval delays," *IEEE Transactions on Power Systems*, vol. 31, no. 4, pp. 3309-3317, July 2016. [click]

[4] P. Shi, Y. Zhang, M. Chadli, and R. K. Agarwal, "Mixed H-infinity and passive filtering for discrete fuzzy neural networks with stochastic jumps and time delays," *IEEE Transactions on Neural Networks and Learning Systems*, vol. 27, no. 4, pp. 903-909, April 2016. [click]

[5] M. Wang, J. Qiu, M. Chadli, and M. Wang, "A switched system approach to exponential stabilization of sampled-data T-S fuzzy systems with packet dropouts," *IEEE Transactions on Cybernetics*, vol. 46, no. 12, pp. 3145 -3156, December 2016. [click]

[6] X. Zhao, C. Ma, X. Xing, and X. Zheng, "A stochastic sampling consensus protocol of networked Euler-Lagrange systems with application to two-link manipulator," *IEEE Transactions on Industrial Informatics*, vol. 11, no. 4, pp. 907-914, August 2015. [click]

[7] K. E. Arzen, "A simple event-based PID controller," *Proceedings of the 14th IFAC World Congress*, Beijing, China, pp. 423-428, 1999.

[8] F. Li, J. Fu, and D. Du, "An improved event-triggered communication mechanism and $\mathcal{L}_\infty$ control co-design for network control systems," *Information Sciences*, vol. 370, pp. 743-762, November 2016. [click]

[9] P. Tabuada, "Event-triggered real-time scheduling of stabilizing control tasks," *IEEE Transactions on Automatic Control*, vol. 52, no. 9, pp. 1680-1685, September 2007. [click]

[10] C. Peng, S. Ma, and X. Xie, "Observer-based non-PDC control for networked T-S fuzzy systems with an event-triggered communication," *IEEE Transactions on Cybernetics*, vol. PP, no. 99, pp. 1-9, May 2017.

[11] C. Peng, J. Li, and M. R. Fei, "Resilient event-triggered H_∞ load frequency control for networked power systems with energy-limited DoS attacks," *IEEE Transactions on Power Systems*, vol. PP, no. 99, pp. 1-9, December 2016.

[12] K. Astrom and B. Bernhardsson, "Comparison of Riemann and Lebesgue sampling for first order stochastic systems," in *Proceedings of the IEEE Conference on Decision and Control*, Las Vegas, United States, pp. 2011-2016, 2002.

[13] M. Mazo and M. Cao, "Asynchronous decentralized event-triggered control," *Automatica*, vol. 50, no. 12, pp. 3197-3203, December 2014. [click]

[14] M. Sigurani, C. Stocker, L. Grune, and J. Lunze, "Experimental evaluation of two complementary decentralized event-based control methods," *Control Engineering Practice*, vol. 35, pp. 22-34, February 2015. [click]

[15] J. Lunze and D. Lehmann, "A state-feedback approach to event-based control," *Automatica*, vol. 46, no. 1, pp. 211-215, January 2010. [click]

[16] X. Meng and T. Chen, "Optimal sampling and performance comparison of periodic and event based impulse control," *IEEE Transactions on Automatic Control*, vol. 57, no. 12, pp. 3252-3259, December 2012. [click]

[17] D. Antunes and W. P. M. H. Heemels, "Rollout event-triggered control: beyond periodic control performance," *IEEE Transactions on Automatic Control*, vol. 59, no. 12, pp. 3296-3311, December 2014. [click]

[18] W. P. M. H. Heemels, M. C. F. Donkers, and A. R. Teel, "Periodic event-triggered control for linear systems," *IEEE Transactions on Automatic Control*, vol. 58, no. 4, pp. 847-861, April 2013. [click]

[19] D. Yue, E. Tian, and Q. L. Han, "A delay system method for designing event-triggered controllers of networked control systems," *IEEE Transactions on Automatic Control*, vol. 58, no. 2, pp. 475-481, February 2013. [click]

[20] R. Postoyan, P. Tabuada, D. Nei, and A. Anta, "A framework for the event-triggered stabilization of nonlinear systems," *IEEE Transactions on Automatic Control*, vol. 60, no. 4, pp. 982-996, April 2015. [click]

[21] L. Lucinda Li and M. Lemmon, "Weakly coupled event triggered output feedback system in wireless networked control systems," *Discrete Event Dynamic Systems: Theory and Applications*, vol. 24, no. 2, pp. 247-260, June 2014.

[22] X. Zhang and Q. L. Han, "Event-based H_∞ filtering for sampled-data systems," *Automatica*, vol. 51, pp. 55-69, January 2015. [click]

[23] Y. S. Moon, P. Park, W. H. Kwon, and Y. S. Lee, "Delay-dependent robust stabilization of uncertain state-delayed systems," *International Journal of Control*, vol. 74, no. 14, pp. 1447-1455, September 2001. [click]

[24] Z. Yan, G. Zhang, and J. Wang, "Non-fragile robust finite-time H_∞ control for nonlinear stochastic *Itô* systems using neural network," *International Journal of Control, Automation and Systems*, vol. 10, no. 5, pp. 873-882, October 2012.

[25] P. Park, J. W. Ko, and C. Jeong, "Reciprocally convex approach to stability of systems with time-varying delays," *Automatica*, vol. 47, no. 1, pp. 235 -238, January 2011.

[26] X. Zhao, X. Zheng, C. Ma, and R. Li, "Distributed consensus of multiple Euler-Lagrange systems networked by sampled-data information with transmission delays and data packet dropouts," *IEEE Transactions on Automation Science and Engineering*, vol. PP, no. 99, July 2015.

[27] Z. Yan, G. Zhang, and W. Zhang, "Finite-time stability and stabilization of linear *Itô* stochastic systems with state and control-dependent noise," *Asian Journal of Control*, vol. 15, no. 1, pp. 270-281, January 2013. [click]

[28] J. H. Kim, "Note on stability of linear systems with time-varying delay," *Automatica*, vol. 47, no. 9, pp. 2118-2121, September 2011. [click]

[29] X. Zhang and Q. L. Han, "Event-triggered dynamic output feedback control for networked control systems," *IET Control Theory and Applications*, vol. 8, no. 4, pp. 226-234, February 2014. [click]

[30] S. Hu and D. Yue, "Event-triggered control design of linear networked systems with quantizations," *ISA Transactions*, vol. 51, no. 1, pp. 153-162, January 2012.

[31] M. C. F. Donkers and W. P. M. H. Heemels, "Output-based event-triggered control with guaranteed $\mathcal{L}_\infty$ gain and improved and decentralized event-triggering," *IEEE Transactions on Automatic Control*, vol. 57, no. 6, pp. 1362-1376, June 2012. [click]

[32] H. Yu and P. J. Antsaklis, "Event-triggered output feedback control for networked control systems using passivity: achieving $\mathcal{L}_2$ stability in the presence of communication delays and signal quantization," *Automatica*, vol. 49, no. 1, pp. 30-38, January 2013.

Fuqiang Li received the Ph.D. degree in Control Theory and Control Engineering from Shanghai University in 2016. He is a postdoctoral researcher in Shanghai University. He is also an associate professor in Henan Agricultural University. His research interests include networked control system and event-triggered control system.

Lisai Gao received the M.S. degree in Control Theory and Control Engineering from Zhengzhou University in 2011. She is a senior engineer. She is currently a Ph.D. candidate in Control Theory and Control Engineering at Shanghai University. Her research interests include networked control systems.

Gensheng Dou received the M.S. degree in Electronics and Communications Engineering from PLA Information Engineering University in 2010. He is a lecturer in Henan Agricultural University. His research interests include hybrid system and networked control system.

Baozhou Zheng received the M.S. degree in Control Theory and Control Engineering from Zhengzhou University in 2006. He is a lecturer in Henan Agricultural University. His research interests include complex system control and event-triggered control system.